Exact diagonalization studies of inelastic light scattering in self-assembled quantum dots

Alain Delgado,[1] Adriel Domínguez,[2] Ricardo Pérez,[3] D. J. Lockwood,[4] and Augusto González[5]
[1]*Centro de Aplicaciones Tecnológicas y Desarrollo Nuclear, Calle 30 No 502, Miramar, Ciudad Habana, CP 11300, Cuba*
[2]*Instituto Superior de Tecnologías y Ciencias Aplicadas, Quinta de los Molinos, Ciudad Habana, CP 10600, Cuba*
[3]*Department of Engineering Physics, McMaster University, Ontario, Canada L8S 4L7*
[4]*Institute for Microstructural Sciences, National Research Council, 1200 Montreal Road, Ottawa, Ontario, Canada K1A 0R6*
[5]*Instituto de Cibernética, Matemática y Física, Calle E 309, Vedado, Ciudad Habana, CP 10400, Cuba*
(Received 22 December 2008; revised manuscript received 23 March 2009; published 20 May 2009)

We report exact-diagonalization studies of inelastic light scattering in few-electron quantum dots under the strong-confinement regime characteristic of self-assembled dots. The spectra of intraband excitations of dots with $N_e=2$, 3, 4, 5, and 6 electrons are calculated. Collective charge-density and spin-density excitations of the systems are identified by computing the multipolar transition amplitudes and the total spin of each excited state of the dots. We apply the orthodox (second-order) theory for scattering due to electronic excitations. Our numerical results stress the dominance of monopole peaks in Raman spectra and the breakdown of selection rules in open-shell dots. The dependence of these spectra on the number of electrons in the dot and the incident photon energy is explicitly shown. Qualitative comparisons are made with recent experimental results.

DOI: 10.1103/PhysRevB.79.195318 PACS number(s): 78.30.−j, 73.21.La, 78.67.Hc

I. INTRODUCTION

Raman spectroscopy is a powerful tool in the investigation of the electronic properties of nanostructures.[1] In a standard experiment, the energy of the incident light beam is slightly above the structure band gap (resonant conditions), and the scattered light is collected in the backward direction (backscattering geometry). Because of the fact that there are two photons involved in a Raman process, selection rules hold for the total angular momentum (or parity) of the electronic subsystem ($\Delta J=0, \pm 2$). These selection rules are different from the rules governing intraband absorption ($\Delta J = \pm 1$, Kohn theorem), thus Raman spectroscopy allows us to study a different sector of the spectrum of electronic excitations in the dot.

In the last few years, Raman measurements in self-assembled quantum dots were reported.[2–4] The distinctive features of these experiments are the observation of peaks, apparently violating the selection rules,[3] and the observation of a strong electron-LO phonon coupling (polaron effect[5]) in self-assembled dots.[4] The description of these effects requires a higher-order theoretical scheme,[6] in which parity-violating vertices are included, in addition to the two electron-photon vertices. We notice, however, that exact calculations for Raman scattering in few-electron quantum dots, even in the lowest- (second-) order scheme, are lacking. To the best of our knowledge, only a few calculations for etched dots are available,[7,8] in which the final states are properly treated, but the intermediate states are not. We think that a precise understanding of the standard Raman-scattering processes in few-electron quantum dots is needed as a basis toward the description of higher-order processes.

Thus, in the present paper we recall the orthodox (standard) second-order Raman scheme for light scattering by electronic excitations in self-assembled quantum dots. We consider dots with up to six electrons. The needed wave functions to compute the Raman cross sections are obtained by exact diagonalization in a truncated basis set of many-particle functions. Because of the resonant character of the process, the intermediate states have an additional electron-hole pair. It means that the largest system we should diagonalize is made up from seven electrons and one hole. The strong-confinement regime, characteristic of self-assembled dots, makes it possible to reach convergence in the numerical calculations with a relatively reduced basis set (of around 10^5 functions). We use the Lanczos algorithm in order to obtain the low-energy spectrum of our Hamiltonian.

The plan of the paper is as follows. In the next section, we present the model quantum dot and the way we compute the Raman transition amplitude. In Sec. III, the intraband excitations of the quantum dot (the final states in a Raman process) are described. A criterium for the "collective" character of a many-particle state is given, which is based on the multipole operators appearing in the off-resonance asymptotics for the Raman amplitude.[9] In that section, we may appreciate how the collective and single-particle excitations shift in energy as the particle number or the confinement strength is varied. In addition, we appreciate how, for open-shell dots, states which are undoubtedly charge excitations give nonzero matrix elements of multipole "spin" operators. Next, in Sec. IV the interband excitations are constructed. They are the intermediate states in a Raman event. We compute the interband absorption to get an idea of the position of the incoming resonances in Raman scattering. In Sec. V, we present the Raman spectra. As it will be shown, the spectra are dominated by monopole peaks, both in polarized and depolarized geometries. This is in accord to the fact that the dot lateral dimensions (~20 nm) are shorter than 1/10 of the light wavelength. Particularly interesting is the observed breakdown of the Raman selection rules in open-shell dots. Finally, in the last section, we qualitatively discuss the relevance of our calculations to the experiments detailed in Refs. 2–4.

II. FORMALISM

The values of the parameters used in our model for self-assembled quantum dots are motivated by the experiments in

Refs. 2–4. For the electron mass and dielectric constants we took, respectively, the following InAs values:[10] $m_e = 0.024 m_0$, and $\epsilon = 14.55 \epsilon_0$. The in-plane confinement potential is assumed parabolic, with a characteristic frequency $\hbar\omega_e$ ranging in the interval between 20 and 50 meV. This is, of course, a simplification. The actual confinement potential is expected to become flat already at excitation energies around 100 meV.[3,4] We will study dots in which the number of electrons varies between 2 and 6.

Under resonance conditions, the Raman-scattering transition amplitude is given by the following expression,[9,11–13] coming from second-order perturbation theory in the scattering matrix,

$$A_{fi} \sim \sum_{\text{int}} \frac{\langle f|H^{(+)}|\text{int}\rangle\langle \text{int}|H^{(-)}|i\rangle}{h\nu_i - (E_{\text{int}} - E_i) + i\Gamma_{\text{int}}}. \quad (1)$$

$h\nu_i$ is the incident laser energy. The initial state in the process is the ground state of the N_e-electron system, meaning that we are considering a process at low temperatures, where only the ground state is populated and hence only Stokes lines in the Raman spectra should be observed. The final states in the process, on the other hand, are quantum dot intraband excitations. Details on how the final states are computed, what their properties are, etc. are given in the next section. We notice that conservation of energy leads to the following relation,

$$E_f - E_i = h\nu_i - h\nu_f, \quad (2)$$

allowing us to express the Raman shift [right-hand side (rhs) of Eq. (2)] in terms of the final-state excitation energy. Varying $h\nu_i$, a peak at a fixed Raman shift (a resonance) indicates the existence of a final state (or group of states) with a given excitation energy. That is how Raman spectroscopy works.

Equation (1) contains a sum over intermediate electronic states. The (virtual) transitions to the intermediate states are caused by the electron-photon interactions. Because of the denominator in Eq. (1), when $h\nu_i$ is slightly above the dot effective band gap the sum is dominated by the resonant terms, i.e., intermediate states with an additional electron-hole pair, whose energies are $E_{\text{int}} - E_i \approx h\nu_i$. They are described in Sec. IV. The intermediate states play, of course, a role in A_{fi}. Incoming and outgoing resonances, i.e., increase in Raman intensities for precise values of $h\nu_i$ or $h\nu_f$, are a consequence of resonances with given intermediate states. However, the position of peaks in Raman spectra is determined solely by the final states. Notice that our expression [Eq. (1)] differs from that one used in Refs. 7 and 8 precisely in the treatment of the intermediate states, which we consider as many-particle and Coulomb interacting states. This allows us to correctly describe incoming and outgoing resonances in Raman scattering.

The electron-photon vertices entering Eq. (1), $H^{(-)}$ and $H^{(+)}$, are single-particle operators in which matrix elements over photon operators were explicitly computed. The − and + supraindexes refer to absorption or emission of a photon, respectively. $H^{(-)}$, for example, is given by

$$H^{(-)} = \sum_{\boldsymbol{\sigma}\boldsymbol{\tau}} \langle \boldsymbol{\sigma}|e^{i\vec{q}_i\cdot\vec{r}}\vec{\epsilon}_i \cdot \vec{p}|\overline{\boldsymbol{\tau}}\rangle e^\dagger_{\boldsymbol{\sigma}} h^\dagger_{\boldsymbol{\tau}}, \quad (3)$$

where we use a basis of two-dimensional (2D) oscillator states, $\boldsymbol{\sigma}$ and $\boldsymbol{\tau}$, for electrons and holes.[14] $\vec{q}_i$ and $\vec{\epsilon}_i$ are the wave vector and polarization of the incident photon. Notice that the electron state in the valence band, $\overline{\boldsymbol{\tau}}$ (conjugate of the hole state $\boldsymbol{\tau}$), enters the matrix element in $H^{(-)}$.

For $H^{(+)}$, we use the relation:

$$\langle f|H^{(+)}|\text{int}\rangle = \langle \text{int}|H^{(-)}|f\rangle^*|_{\vec{q}_f,\vec{\epsilon}_f}, \quad (4)$$

where the matrix element in the rhs is to be evaluated with the wave vector and polarization of the scattered photon.

III. INTRABAND EXCITATIONS IN SELF-ASSEMBLED DOTS

Self-assembled quantum dots may have quite different shapes depending on the growth conditions.[15] However, in Ref. 16 the authors proposed a new procedure for the growth of stacked self-assembled dots whose main effect is to convert the quantum dot population in a population of quantum disks. In our model, we assume a disk-shaped structure of around 20 nm diameter and 5 nm high. The motion of electrons along the axis (z direction) is quantized, occupying the first subband. For the motion in the perpendicular plane, we use a harmonic-oscillator potential.

In order to compute the intraband excitations of the N_e-electron quantum dot we diagonalize the electronic Hamiltonian,

$$H = \sum_{\boldsymbol{\sigma}} (E_z^{(e)} + \hbar\omega_e \varepsilon_{\boldsymbol{\sigma}}) e^\dagger_{\boldsymbol{\sigma}} e_{\boldsymbol{\sigma}} + \frac{\beta}{2} \sum_{\boldsymbol{\lambda}\boldsymbol{\mu}\boldsymbol{\sigma}\boldsymbol{\tau}} \langle \boldsymbol{\lambda}, \boldsymbol{\mu}|\frac{1}{r_{12}}|\boldsymbol{\sigma}, \boldsymbol{\tau}\rangle e^\dagger_{\boldsymbol{\lambda}} e^\dagger_{\boldsymbol{\mu}} e_{\boldsymbol{\tau}} e_{\boldsymbol{\sigma}}, \quad (5)$$

in a basis of Slaters determinants. In Eq. (5), $E_z^{(e)} = \hbar^2\pi^2/(2m_e L_z^2)$, and $L_z = 5$ nm is the dot width. The energy of 2D oscillator states is $\varepsilon_{\boldsymbol{\sigma}} = 2k_{\boldsymbol{\sigma}} + |l_{\boldsymbol{\sigma}}| + 1$, where k is the radial quantum number, and l is the angular momentum along the normal to the plane. The matrix elements of Coulomb interactions, $\langle \boldsymbol{\lambda}, \boldsymbol{\mu}|1/r_{12}|\boldsymbol{\sigma}, \boldsymbol{\tau}\rangle$, among any four states of the first 20 oscillator shells were computed and stored in a file. The strength of Coulomb interactions is given by $\beta = e^2/(4\pi\epsilon l_e)$, where e is the electron charge, and l_e the electron oscillator length. With the explicit values of the parameters, we get $\beta = 1.75\sqrt{\hbar\omega_e}$ meV, where $\hbar\omega_e$ is to be written in meV also. Notice that the ratio between characteristic Coulomb and oscillator energies, $\beta/\hbar\omega_e$, is less than one for self-assembled dots (around 0.25 for $\hbar\omega_e = 50$ meV).

The dimension of the Hamiltonian matrix can be reduced by restricting the basis to sectors with given values of the total angular momentum, $L = \Sigma_{\boldsymbol{\sigma}} l_{\boldsymbol{\sigma}}$, and total spin projection, $S_z = \Sigma_{\boldsymbol{\sigma}} s_{z\boldsymbol{\sigma}}$. The dimension is further reduced by introducing an energy cutoff. Due to the strong confinement, we obtain converged eigenvalues of Hamiltonian (5) using a truncated basis of Slater determinants with zeroth-order (harmonic oscillator) excitation energy lower than $8\hbar\omega_e$. This leads to matrices with dimensions less than 10^4 which are easily diagonalized. The algorithm used in our Fortran 90 code has

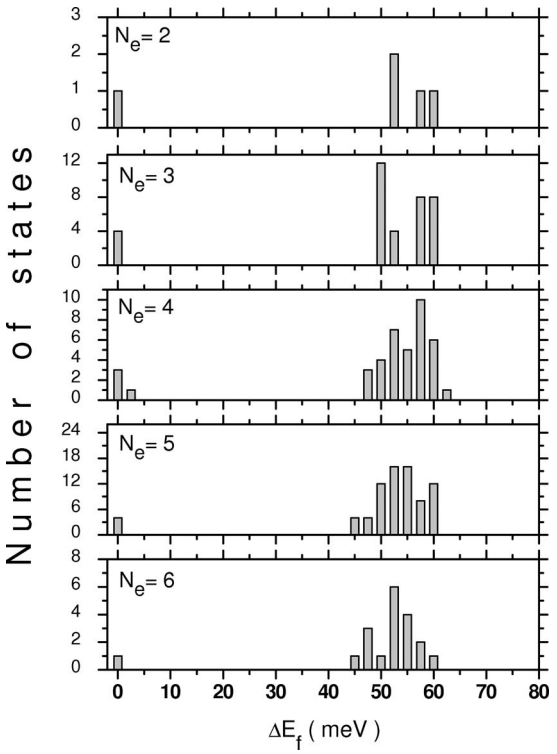

FIG. 1. Density of energy levels in few-electron dots for $\hbar\omega_e = 30$ meV and excitation energy below 100 meV. See explanation in the text.

many similarities with published ones.[17–19] It is not yet parallelized, although it may be easily adapted for parallel computation.

A sample of the results is shown in Fig. 1 for dots with $N_e=2-6$, and $h\omega_e=30$ meV. In this figure, we present the density of energy levels for the excited states with the same L and S_z as the ground states. These are the final states giving the main contribution to the Raman cross section. Notice the ground-state degeneracies in the $N_e=3$ dot (quantum numbers: $L=\pm 1$, $S_z=\pm 1/2$), in the $N_e=4$ dot ($L=0$, $S_z=0,\pm 1$), and in the $N_e=5$ dot ($L=\pm 1$, $S_z=\pm 1/2$). The width we use to construct the histograms is 0.4 meV. This value is close to the mean spacing between levels in the calculated quantum dots.

A more detailed view of the spectrum of excited states in the six-electron dot is drawn in Fig. 2. This is a closed-shell system with ground-state quantum numbers $L_i=S_i=0$. Using a common terminology,[12] we will refer to $\Delta L=L_f-L_i=0$ states as monopole excitations, $\Delta L=\pm 1$ states as dipole excitations, $\Delta L=\pm 2$ states as quadrupole excitations, etc. On the other hand, states with total spin variation, $\Delta S\neq 0$, will be called spin excitations, even if $\Delta S_z=0$, in contrast to charge excitations which correspond to $\Delta S=0$. The cases $\Delta S_z\neq 0$ (spin flips) will not be considered below because the Raman amplitudes for transitions to such states are very small.[12,13] Spin-flip peaks in the Raman spectra are the result of higher-order processes and will not be studied in the present paper.

In Fig. 2, collective states are also indicated. We identify them with the help of sum rules. Sum rules form a very

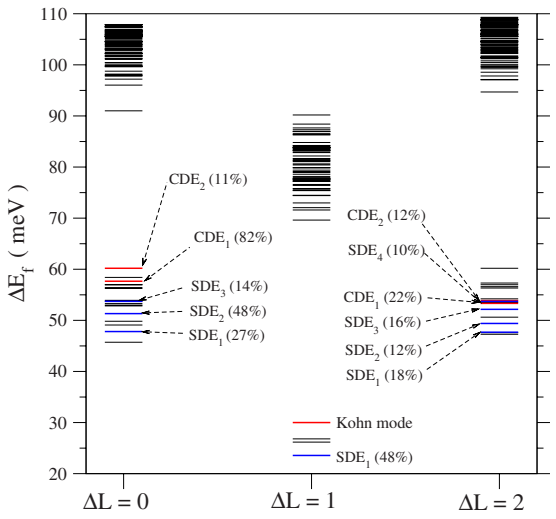

FIG. 2. (Color online) The low-lying intraband excitations in the six-electron quantum dot. $\hbar\omega_e=30$ meV. The relative contribution to energy-weighted sum rules of collective states is given.

important tool in the theory of collective excitations.[20] In many cases, they allow a calculation of global properties in a simple way and are therefore useful in testing different approximation schemes. In general, a sum rule is related to a single-particle operator $D=\Sigma d_{\alpha\beta}e^{\dagger}_{\alpha}e_{\beta}$. It gives the kth moment of the distribution of the excitation strength produced by the one-body operator D,

$$S_k \equiv \sum_f (E_f - E_i)^k (|\langle f|D|i\rangle|^2 + |\langle f|D^{\dagger}|i\rangle|^2). \tag{6}$$

The most important sum rule is the energy-weighted sum rule (EWSR) S_1. The EWSR for charge excitations is written as follows:

$$\sum_f \Delta E_f \{|\langle f|D^{(c)}_{\Delta L}|i\rangle|^2 + |\langle f|D^{(c)\dagger}_{\Delta L}|i\rangle|^2\} = \langle i|[D^{(c)}_{\Delta L},[H,D^{(c)\dagger}_{\Delta L}]]|i\rangle. \tag{7}$$

Relation (7) holds for a set of exact eigenvalues $|f\rangle$ of H. We usually have only approximative states $|f\rangle$ and approximative energies E_f. We have already shown that the right-hand side of Eq. (7) can be calculated in a rather simple way.[21] It is a test of the validity of any approximation to see whether it fulfills the sum rules.

In our scheme, a state $|f\rangle$ will be conventionally called collective [a charge-density excitation (CDE)] if $\Delta E_f|\langle f|D^{(c)}_{\Delta L}|i\rangle|^2$ is greater than 5% of the rhs of Eq. (7). In contrast, a state with a small contribution to the sum rule is called a single-particle excitation (SPE). The multipole operator is defined as

$$D^{(c)}_{\Delta L} = \sum_{\boldsymbol{\lambda},\boldsymbol{\mu}} \langle \boldsymbol{\lambda}|d_{\Delta L}|\boldsymbol{\mu}\rangle e^{\dagger}_{\boldsymbol{\lambda}}e_{\boldsymbol{\mu}}, \tag{8}$$

where the sum runs over oscillator states $\boldsymbol{\lambda}$ and $\boldsymbol{\mu}$ with the same spin projection. The matrix elements $\langle \boldsymbol{\lambda}|d_{\Delta L}|\boldsymbol{\mu}\rangle$ are given elsewhere.[13,21] Making explicit the spin degrees of freedom, we write

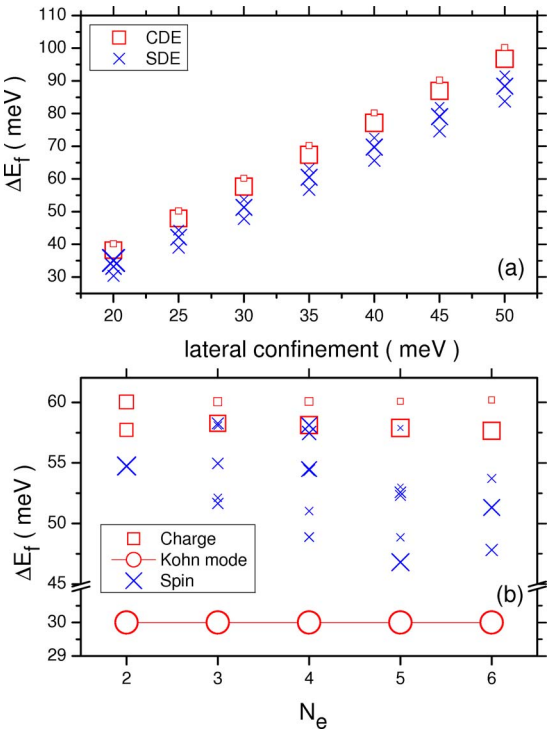

FIG. 3. (Color online) (a) Collective monopole excitations below 100 meV in the six-electron dot as a function of $\hbar\omega_e$. (b) Sum-rule fractions for monopole states in the few-electron dots and a confinement potential with $\hbar\omega_e$=30 meV. The Kohn mode (dipole excitation) is also drawn as a reference.

$$D_{\Delta L}^{(c)} = \sum_{\lambda,\mu} \langle \lambda | d_{\Delta L} | \mu \rangle (e_{\lambda\uparrow}^{\dagger} e_{\mu\uparrow} + e_{\lambda\downarrow}^{\dagger} e_{\mu\downarrow}), \tag{9}$$

in which λ and μ now refer to orbital functions (no spin). These operators $D_{\Delta L}^{(c)}$ enter the asymptotic expression for the Raman amplitude in the off-resonance regime.[9] They are multiplied by the scalar product, $\vec{\epsilon}_i \cdot \vec{\epsilon}_f$, between the incident and scattered light polarization vectors.

On the other hand, a second term in the asymptotic off-resonance expression,[9] proportional to $(\vec{\epsilon}_i \times \vec{\epsilon}_f) \cdot \hat{z}$, involves the operator,

$$D_{\Delta L}^{(s)} = \sum_{\lambda,\mu} \langle \lambda | d_{\Delta L} | \mu \rangle (e_{\lambda\uparrow}^{\dagger} e_{\mu\uparrow} - e_{\lambda\downarrow}^{\dagger} e_{\mu\downarrow}). \tag{10}$$

This operator may serve to distinguish collective spin excitations [spin-density excitations (SDE)] only when the ground-state total spin is S_i=0. When $S_i \neq 0$, the correspondence is not unique, meaning that we could observe peaks corresponding to charge excitations in the cross-polarized Raman spectrum of open-shell dots.

Notice that, in Fig. 2, the dipolar SDEs are the lowest states in that sector, and the monopole CDEs are at the top of the first group of monopole states, having excitation energies roughly equal to $2\hbar\omega_e$.

Figure 3(a) shows the collective states of the six-electron dot as a function of the confinement strength, $\hbar\omega_e$. States have been denoted by symbols, whose sizes are proportional to their weight in the corresponding sum rule.

On the other hand, in the lower panel of Fig. 3, the harmonic energy is fixed at $\hbar\omega_e$=30 meV, and the monopole states with fractions of the charge or spin sum rules higher than 5% are drawn as a function of the number of electrons in the dot. There is a remarkable fact in these dots, working under the strong-confinement regime, related to the position of the main CDE state: it is almost independent of the number of electrons in the dot. We shall comment further on this fact with the help of the explicit values of the sum-rule fractions given in Table I.

The main collective charge excitations, CDE_1 and CDE_2, correspond, respectively, to excitations of the internal motion and center-of-mass Hamiltonians. The energy of CDE_2 should be exactly $2\hbar\omega_e$ according to the Kohn theorem. However, CDE_1 shows also very little dependence on N_e and, as seen from the table, gives stronger contributions to the sum rule, meaning that it should dominate the Raman spectrum in the off-resonance regime.

A second point to stress in Table I is related to the open-shells dots, where charge-density excitations may contribute not only to the charge EWSR, but also to the spin EWSR. That is, in an off-resonance regime the Raman peaks associated to these modes could appear in both, polarized and depolarized spectra. This is a clarifying result since usually Raman peaks appearing in both geometries were attributed to single-particle excitations. This fact is related to the spin-wave functions of the states and the operator given by Eq. (10). Notice also the triplet-to-singlet spin density transitions in the four-electron dot.

IV. INTERBAND EXCITATIONS

The intermediate states entering Eq. (1) for the transition amplitude are interband excitations of the dot, i.e., states with an additional electron-hole pair. We will use a simplified description with only one (heavy) hole band with effective anisotropic mass, $m_h^{(z)}=0.35m_0$, $m_h^{(xy)}=0.035m_0$.[10] This is not a very crude hypothesis, which may be justified to work in the conditions of self-assembled dots because of the shift of light-hole states due to the small width of the dots along the symmetry axis. Indeed, when L_z=5 nm, light-hole states are 0.5 eV higher in energy than heavy-hole states.

Under this simplification, the intermediate states are characterized by the total angular momentum, L_{int}, the hole spin projection, $S_z^{(h)}$, and the total electronic spin projection, $S_z^{(e)}$. The main contribution to the Raman amplitude comes from states in which the added pair has angular momentum equal to zero, that is $L_{\text{int}}=L_i$, where L_i is the initial (ground-) state angular momentum of the N_e-electron system.

We should then diagonalize Hamiltonian (5) with two additional terms,

$$\sum_{\boldsymbol{\sigma}} (E_z^{(h)} + \hbar\omega_h \varepsilon_{\boldsymbol{\sigma}}) h_{\boldsymbol{\sigma}}^{\dagger} h_{\boldsymbol{\sigma}} - \beta \sum_{\boldsymbol{\lambda}\boldsymbol{\mu}\boldsymbol{\sigma}\boldsymbol{\tau}} \langle \boldsymbol{\lambda}, \boldsymbol{\mu} | \frac{1}{r_{12}} | \boldsymbol{\sigma}, \boldsymbol{\tau} \rangle e_{\boldsymbol{\lambda}}^{\dagger} h_{\boldsymbol{\mu}}^{\dagger} h_{\boldsymbol{\tau}} e_{\boldsymbol{\sigma}}, \tag{11}$$

the first one represents the single-particle energy of the hole, and the second one accounts for the electron-hole interactions. We assume that the oscillator length for holes is equal

TABLE I. The sum-rule fractions represented in Fig. 3(b). $S_1^{(c,s)}$ refer, respectively, to the charge and spin energy-weighted sum-rule fractions. Charge-excitation states giving only contributions to the spin sum rule are denoted CEs.

$N_e=2$, $L=0$, $S=0$	ΔE_f (meV)	$S_1^{(c)}$	$S_1^{(s)}$	ΔS
SDE_1	54.74	0%	96%	+1
CDE_1	57.72	43%	0%	0
CDE_2	60.03	51%	0%	0
$N_e=3$, $L=\pm1$, $S=1/2$	ΔE_f (meV)	$S_1^{(c)}$	$S_1^{(s)}$	ΔS
SDE_1	51.65	0%	21%	+1
SDE_2	52.11	0%	10%	+1
CE_1	54.96	0%	22%	0
CE_2	58.08	0%	11%	0
CDE_1	58.27	69%	23%	0
CDE_2	60.05	26%	0%	0
$N_e=4$, $L=0$, $S_z=\pm1$	ΔE_f (meV)	$S_1^{(c)}$	$S_1^{(s)}$	ΔS
SDE_1	48.88	0%	16%	+1
CE_1	51.02	0%	11%	0
CE_2	54.41	0%	22%	0
CDE_1	58.13	80%	41%	0
CDE_2	60.07	18%	5%	0
$N_e=4$, $L=0$, $S_z=0$	ΔE_f (meV)	$S_1^{(c)}$	$S_1^{(s)}$	ΔS
SDE_1	48.88	0%	20%	+1
SDE_2	54.48	0%	41%	−1
SDE_3	57.47	0%	33%	−1
$N_e=5$, $L=\pm1$, $S=1/2$	ΔE_f (meV)	$S_1^{(c)}$	$S_1^{(s)}$	ΔS
SDE_1	46.80	0%	6%	+1
SDE_2	48.86	0%	12%	+1
SDE_3	52.31	0%	20%	+1
CE_1	52.58	0%	23%	0
SDE_4	53.03	0%	7%	+1
CDE_1	57.88	84%	6%	0
CDE_2	60.08	11%	0%	0
$N_e=6$, $L=0$, $S=0$	ΔE_f (meV)	$S_1^{(c)}$	$S_1^{(s)}$	ΔS
SDE_1	47.81	0%	27%	+1
SDE_2	51.31	0%	48%	+1
SDE_3	53.72	0%	14%	+1
CDE_1	57.65	82%	0%	0
CDE_2	60.19	11%	0%	0

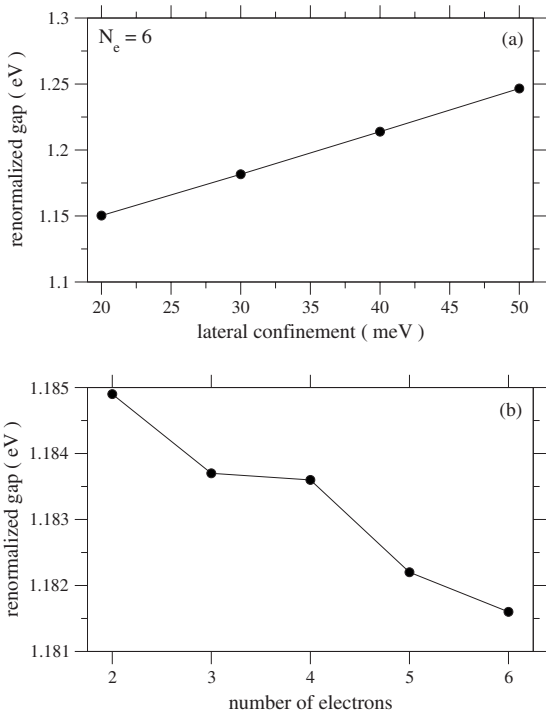

FIG. 4. (a) The effective band gap in the six-electron dot as a function of $\hbar\omega_e$. (b) Band gap in the few-electron dots for a confinement potential with $\hbar\omega_e=30$ meV.

to the electron oscillator length, i.e., $m_e\omega_e=m_h\omega_h$. The basis functions are built up as products of Slater determinants for electrons and a single harmonic-oscillator function for the hole. As in the previous section, we define the excitation energy for these functions in terms of the difference of zero-order (harmonic-oscillator) energies. The reference is the lowest energy in the basis. With a cutoff of $8\hbar\omega_e$ for the excitation energy (enough to reach convergence), matrix dimensions of around 10^5 are obtained. The lowest 100 eigenvalues are easily computed by means of Lanczos algorithms.[22]

We show in Fig. 4 the gap renormalization effects in the dots as a result of varying the confinement strength or the number of electrons. The renormalized gap is simply the energy difference between the lowest intermediate state and the ground state in the dot. Notice that the effective gap (around 1.18 eV) is the result of adding a nominal $E_{\text{gap}}=0.43$ eV, the confinement energies along the z direction of the added electron and hole $(E_z^{(e)}+E_z^{(h)})$, the in-plane confinement energies of both particles, and the contribution from Coulomb interactions. The dependence on $\hbar\omega_e$ is almost linear, as expected, because of the single-particle terms in the Hamiltonian. The small redshift of the effective band gap with increasing N_e, on the other hand, comes from the prevalence of electron-hole attractive interactions over phase-space filling effects in small dots.

In Fig. 5, we show the interband absorption in dots with $N_e=2,\ldots,6$ and $\hbar\omega_e=30$ meV. The intention is to show possible incoming resonances in Raman-scattering processes. The absorption spectrum at normal incidence is computed from the matrix elements squared, $|\langle \text{int}|H^{(-)}|i\rangle|^2$, smeared out with a Lorentzian. We used a uniform width for

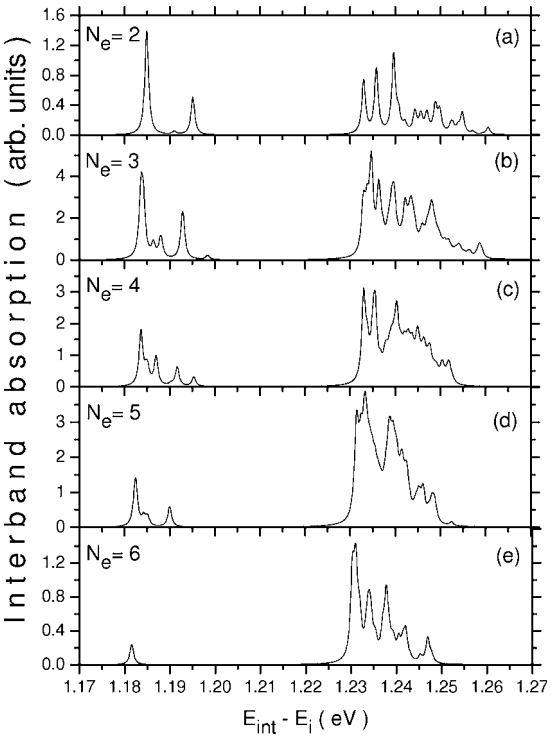

FIG. 5. Interband absorption in the few-electron dots with a confinement potential $\hbar\omega_e$=30 meV. The spectra were calculated assuming a uniform width Γ_{int}=0.5 meV for the intermediate states.

the intermediate states, Γ_{int}=0.5 meV. Only intermediate states with the same angular momentum as the electronic ground states are included in the computation, that is $L_{\text{int}}=L_i$. Two spin combinations are considered $S^{(e)}_{z,\text{int}}=S^{(e)}_{z,i}+1/2$, $S^{(h)}_{z,\text{int}}=-1/2$, and $S^{(e)}_{z,\text{int}}=S^{(e)}_{z,i}-1/2$, $S^{(h)}_{z,\text{int}}=1/2$.

Although $\hbar\omega_e$=30 meV is not the strongest confinement achievable in self-assembled dots, we clearly distinguish in Fig. 5 absorption peaks arranged in shells separated by $2\hbar\omega_e$. The dispersion of peaks in the first shell ranges from 15 meV in the N_e=2 dot to a single (doubly degenerate) peak in the six-electron dot. Incoming resonances in a Raman spectra should be then very sharp if experiments were conduced in a very high quality dot array or a single dot with the use of confocal microscopy.

Specially interesting is the six-electron dot, where an almost ideal Raman process with transitions through a single intermediate resonance at 1181.6 meV can be realized. Results for Raman cross sections are presented in the next section.

V. RAMAN SPECTRA

The first feature of Raman spectra in self-assembled dots is the dominance of monopole (ΔL=0) peaks. This property is shared with etched dots,[12,23] but it is much more accentuated for self-assembled dots because of their smaller dimensions. Indeed, the typical diameter, d, of InAs dots in a GaAs matrix, for example, is around 20 nm. On the other hand, the Raman amplitude squared, $|A_{fi}|^2$ for a state $|f\rangle$ with a given

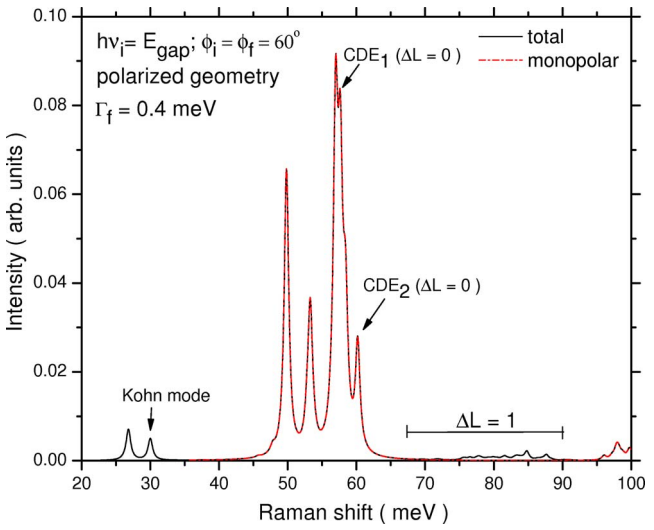

FIG. 6. (Color online) Polarized Raman spectrum for a six-electron dot with confinement $\hbar\omega_e$=30 meV. Monopolar (dashed line) and total (solid line) spectra are drawn. The total cross section includes contributions from monopole, dipole, and quadrupole states.

ΔL is proportional to $(q_i \sin\phi_i d)^{2|\Delta L|}$, where ϕ_i is the angle of incidence of photons, and $q_i \approx 0.006$ nm^{-1} is the wave vector of photons with energy equal to 1.18 eV. The product $q_i d$ is roughly 0.12, meaning that only ΔL=0 peaks should be observed.

We show in Fig. 6 the spectrum for a N_e=6 dot and $\hbar\omega_e$=30 meV. The incident photon energy is exactly in resonance with the first exciton state shown in Fig. 5(e), that is $h\nu_i$=1181.6 meV. The differential cross section is computed from the expression,

$$d\sigma \sim \sum_f |A_{fi}|^2 \frac{\Gamma_f/(4\pi)}{\Gamma_f^2 + (h\nu_f + E_f - E_i - h\nu_i)^2}, \qquad (12)$$

where we used a Lorentzian to smear out the Dirac delta function expressing conservation of energy, Eq. (2). The width of final states, Γ_f, is assumed uniform and equal to 0.4 meV. When the ground state is degenerate, we sum over all of the terms in the multiplet.

The calculations shown in Fig. 6 correspond to the polarized geometry, under backscattering conditions and incidence angle (in vacuum) equal to 60° in order to strengthen multipole peaks. Contributions from ΔL=0 (monopole), $\Delta L=\pm 1$ (dipole), and $\Delta L=\pm 2$ (quadrupole) final-state excitations are included in the sum in Eq. (12). Dipole final states with Raman shifts around 30 meV (in particular, the Kohn mode) and around 80 meV give rise to peaks at least 1 order of magnitude smaller than the leading monopole peaks lying in the interval from 50 to 60 meV. Quadrupole states, present also in this interval (see Fig. 2), give, however, a negligible contribution to the cross section. Notice that, under resonance conditions, peaks associated with single-particle monopole excitations are as strong as the peaks corresponding to the collective states (CDE). Let us stress also that the main Raman peaks are shifted 50–60 meV below the

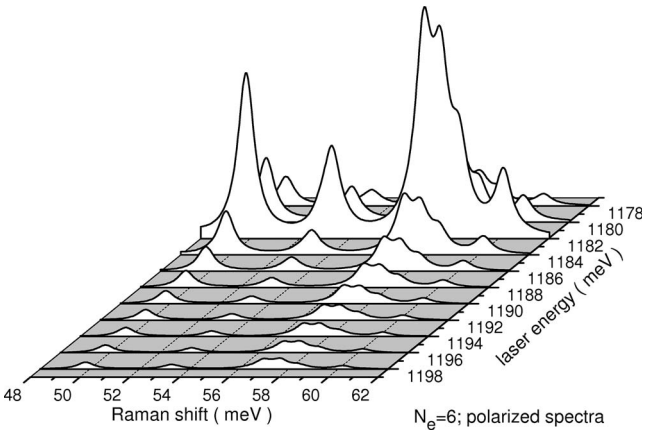

FIG. 7. Polarized Raman spectrum in the six-electron dot as a function of the incident laser energy.

luminescence lines and, for this reason, should be easily observable.

Polarized spectra for the six-electron dot as a function of the incident photon energy, $h\nu_i$, are shown in Fig. 7. The incident angle in this and the next figures is $\phi_i=10°$. Due to the special character of these processes, with transitions through a single intermediate-state resonance, the dependence on $h\nu_i$ is uniform, with a sharp maximum at the resonance. Away from the resonance, on both sides of it, the CDE_1 state gives the strongest peak.

The $N_e=6$ spectra may be contrasted with the $N_e=4$ polarized spectra, shown in Fig. 8. The $h\nu_i$ intervals shown in both figures are the same in order to facilitate comparison. Resonances with different intermediate states (see Fig. 5) lead, in the present case, to a pattern in which the relative intensities of Raman peaks rapidly vary with $h\nu_i$. This is the common feature of all of the studied dots except the $N_e=6$ one. There are also interesting facts about the Raman spin selection rules, but they are more evident in the next figure (Fig. 9), where polarized and depolarized spectra are drawn as a function of N_e.

Monopolar spectra in Fig. 9 are computed at incident photon energy exactly in resonance with $E_{\rm gap}$ of each dot. First,

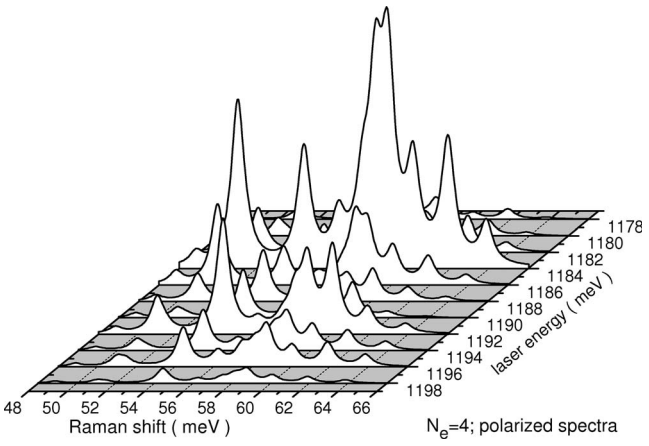

FIG. 8. Polarized Raman spectrum for a four-electron dot with confinement $\hbar\omega_e=30$ meV. The initial photon energy is varied in the interval where the first set of incoming resonances is expected.

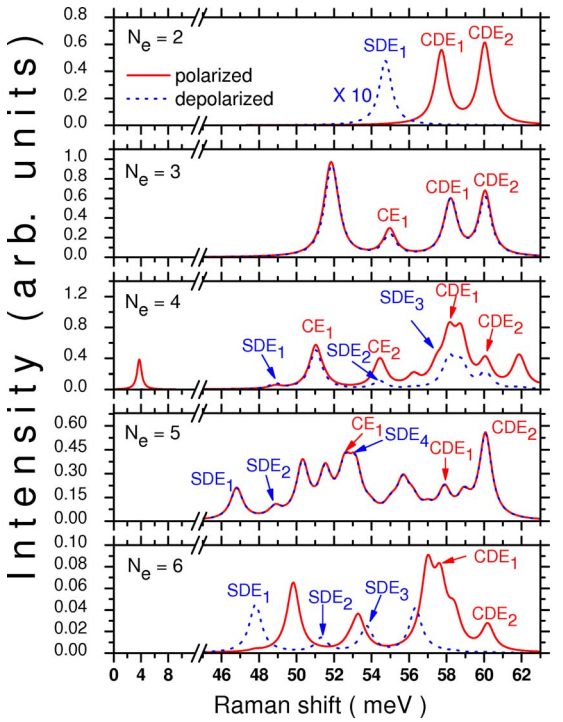

FIG. 9. (Color online) Polarized and depolarized monopolar Raman spectra in the few-electron dots with confinement $\hbar\omega_e=30$ meV. The initial photon energy is exactly in resonance with the first intermediate state ($E_{\rm gap}$) in each dot.

we notice that for the $N_e=2$ and $N_e=6$ (closed-shell) dots, in which the ground-state total electronic spin is $S_i=0$, the spin selection rules deduced in the off-resonance regime (ORA) hold even under resonance conditions.[24] That is, CDEs and SPEs with $\Delta S=0$ are observed in the polarized spectrum, and SDEs and SPEs with $\Delta S=1$ are observed in the depolarized spectrum. This is not the case for the open-shell dots, in particular the $N_e=3$ and 5 dots, for which the polarized and depolarized spectra are very similar, and we cannot use the selection rules in order to identify spin or charge excitations. In the $N_e=4$ dot, we observe the singlet state (a spin excitation), which can be classified as a SPE according to the sum rule, as a distinct low-energy peak in the polarized spectrum. Notice that, in general, the weights in the sum rule given in Table I are not indicative of the relative intensities of peaks in the Raman spectrum. On the other hand, the positions of CDEs states practically do not depend on N_e, specially the CDE_2, as mentioned in the comments to Fig. 3, and the SDEs peaks shift to lower energies as N_e is increased.

Finally, we would like to address the question about outgoing resonances. These resonances are defined by following the intensity of a fixed Raman peak as a function of the energy of the scattered photon. In bulk systems, outgoing resonances associated with collective final states were found at exactly the same energy positions of incoming resonances, which led to the idea that outgoing resonances are a consequence of a third-order process, in which an additional perturbation causes the decay of the intermediate state toward the exciton (incoming resonance).[25] We would like to check what happens when employing exact functions in the standard (second-order) scheme.

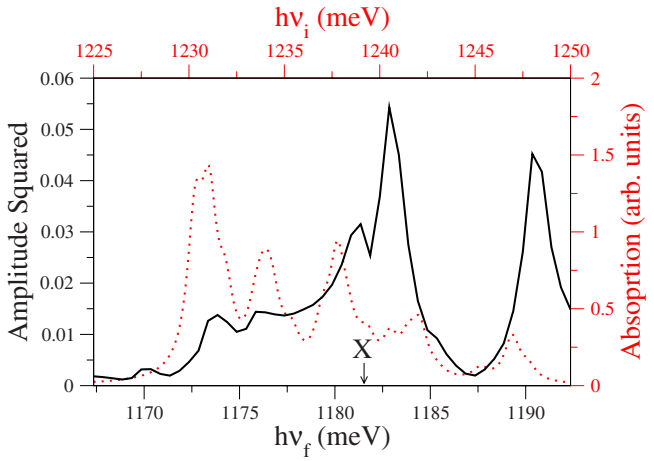

FIG. 10. (Color online) The amplitude squared, $|A_{fi}|^2$, solid line, corresponding to the CDE_1 state in the $N_e=6$ dot and $\hbar\omega_e=30$ meV as a function of the scattered photon energy, $h\nu_f$. The absorption intensity (dashed line) is also shown for comparison. Notice that the x axis in the absorption curve corresponds to $h\nu_i$. The energy of the first incoming resonance is indicated by an arrow.

Figure 10 shows the amplitude squared, $|A_{fi}|^2$, corresponding to the CDE_1 state, that is, the most collective charge-density state, in the $N_e=6$ dot and $\hbar\omega_e=30$ meV, as a function of the scattered photon energy, $h\nu_f$. A strong peak at $h\nu_f \approx 1183$ and 1.4 meV above the energy of the first incoming resonance (indicated by an arrow in the figure), is observed. In our scheme, this means a strong resonance with an intermediate state with energy $E_{\text{int}} \approx E_X + \Delta E(\text{CDE}_1)$, where $E_X=1181.6$ meV is the position of the first absorption maximum (exciton), and $\Delta E(\text{CDE}_1)=E_f(\text{CDE}_1)-E_i$. Comparison with the absorption intensity, also depicted in the figure with a dashed line, shows that the absorption peak is not the strongest for this particular intermediate state. This means that the matrix element corresponding to virtual emission of a photon, $\langle f|H^{(+)}|\text{int}\rangle$, should be particularly strong for this intermediate state, see Eq. (1). We verified a similar situation with regard to the most collective spin-density excitation (the SDE_2). The existence of an intermediate state with such characteristics, energy approximately equal to the sum of two eigenenergies, and a strong transition probability to the collective state, suggest a kind of approximate dynamical symmetry, and requires further research.

VI. QUALITATIVE ANALYSIS OF REPORTED EXPERIMENTS

Although there have been a number of reports of experimental Raman studies dating from the 1990s of deep etched quantum dots with large numbers (hundreds) of electrons (see, for example, Refs. 26–28), apart from two preliminary theoretical studies for 6 and 12 electrons,[29,30] the initial experimental investigations of inelastic light scattering from quantum dots containing few electrons commenced in 2000. In that year Chu *et al.*[2] observed at 5 K under resonance excitation from self-assembled InGaAs/GaAs quantum dots a Raman peak near 50 meV with a linewidth of about 25 meV. Similar Raman spectra were observed in both polarized and depolarized scattering conditions without any apparent depolarization shift. From sample doping considerations and other experiments, Chu *et al.* deduced that there were about six electrons in each quantum dot and that the ground- and first-excited state of the dot were occupied. They interpreted the depolarized Raman peak as arising from SDEs while the polarized peak was associated with charge-density fluctuations. Despite the lack of the expected fine structure in their reported spectrum because of energy-level variations in the conduction band arising from a statistical distribution of dot diameters in their sample,[2] our calculations do confirm this assignment. As mentioned in Sec. V and shown in Fig. 6, monopole Raman scattering dominates in few electron dots at resonance and the Raman spectrum of a closed-shell dot containing six electrons should exhibit a clear difference between SDEs in the depolarized scattering geometry and CDEs in polarized scattering. This was not the case in Chu *et al.*'s work. On the other hand, for five, but not four, electrons contained in the dot, the polarized and depolarized spectra are expected to be very similar. Thus the broad 50 meV peak observed by Chu *et al.*, which covers the right energy range according to our theory for a confinement energy of 30 meV, is definitely electronic in origin, is due to intersublevel transitions within the conduction band, and is well explained by taking five instead of six electrons in their dots.

In 2003, Brocke *et al.*[3] investigated the electronic excitations in InGaAs/GaAs self-assembled quantum dots where the dots could be filled with from one to six electrons by varying a gate voltage across the dots. Their resonant Raman-scattering experiments revealed a broad Raman band in the energy range 40–55 meV in the polarized geometry (there was not mention of the depolarized spectrum in this paper). A feature of their results was the prominent peak observed at ~50 meV (linewidth of ~5 meV) for two electrons in the dots that was assigned to a CDE. This peak was seen to gradually shift to lower energy (~46 meV for six electrons) with increasing number of electrons in the dots. The shift was opposite in direction to their expectations for CDEs and was explained in terms of the Coulomb interaction among the dot electrons. Apart from the Kohn mode at 50 meV, their energy-level calculations showed the existence of other excitations to lower energy (in the range 40–50 meV) for greater than two electrons per dot, but these additional low-energy excitations were not individually resolved in the experiments.[3] No calculated Raman spectra were given in this paper. Without this information, the implication of their energy-level analysis performed using a confinement energy of 50 meV is that the clear peak they observed at ~50 meV for at least two electrons per dot was the Kohn mode. Our calculations of the Raman spectrum although for pure InAs dots with a confinement energy of 30 meV produce Raman peaks in a similar energy range to that observed by Brocke *et al.*, and most importantly show that the $\Delta L=1$ transitions including the Kohn mode at 30 meV give negligible contributions to the Raman intensity under resonance excitation. The present calculations show that in polarized scattering two CDEs spaced by 2–3 meV (CDE_1 and CDE_2 shown in Fig. 9) are prominent, but their energies do not shift much with increasing number of electrons in the dot (see Fig. 3).

Based on these results, we can reinterpret the Raman results of Brocke *et al.* as follows. Their spectra show a peak at ~45 meV and evidence that a similar peak occurs at ~50 meV (this peak is more clearly seen at low and high electron numbers) that do not shift with electron number and are thus likely due to CDEs. The apparent shift of the ~50 meV peak to lower energy with increasing electron number is an illusion created by the appearance of additional Raman peaks at energies between 45 and 50 meV, especially for four and five electrons (see Fig. 9), that are unresolved in the Bocke *et al.* experiments. A more quantitative analysis than this requires further detailed calculations for the specific physical properties of their dot structure.

The experimental results that motivated this theoretical study were obtained recently from resonance Raman-scattering measurements on InAs/GaAs self-assembled quantum dots filled by *n*-type modulation doping with 5, 7, and 12 electrons.[4] Detailed results were published for ~7 electron dots with intersublevel transitions in the ~50 meV range. On resonance excitation a broad electronic Raman line was observed at 57 meV (linewidth ~15 meV) in a near-polarized geometry that was attributed to intersublevel electron transitions. No detailed structure of this Raman band was noted for ~7 electrons,[4] but its peak energy increased slightly with increasing number of dot electrons from 55 meV for ~5 electrons to 63 meV for ~12 electrons, at which point some band structure became evident.[31] As opposed to the Brocke *et al.* results,[3] the apparent peak position of this Raman band increases slightly with the number of electrons per dot and thus is in accord with an assignment to CDEs. Although our calculations for InAs quantum dots extend only to six electrons they show that there are two CDEs expected in the vicinity of the 57 meV peak observed by Aslan *et al.* and they do not shift much in energy with increasing number of electrons. In fact, The calculated polarized monopolar Raman spectrum shown in Fig. 9 for six electrons exhibits a maximum at 57 meV and, when appropriately broadened, resembles quite well the experimentally observed Raman band for ~7 electrons. One additional interesting aspect of the work of Aslan *et al.* was their observation of strong coupling between quantum dot longitudinal-optical phonons and electron intersublevel transitions.[4] Such coupling modifies the signatures of both the phonon and electronic Raman lines and thus for better comparison with experiment further theoretical calculations including the effects of electron-phonon coupling are desirable.

Finally, for completeness, we briefly consider the obverse case of resonant Raman scattering from holes in self-assembled dots. Such scattering has been observed in both SiGe/Si (Ref. 32) and InAs/GaAs (Ref. 33) quantum dots. In the InAs dot work, *p*-type doping resulted in two to five holes per dot depending on the as-grown dot density. Resonant Raman scattering from such samples produced a broad intersublevel hole excitation at ~25 meV (linewidth ~12 meV) for two to three holes per dot that shifted to lower energies with increasing numbers of holes per dot. Detailed theoretical work is needed to explain these results.

In summary, our theoretical results have proved to be in qualitative agreement with experiment. However, in general, not all the detailed structure predicted in our calculations and its polarization dependence for dots filled with from two to six electrons has been observed experimentally, because of the wide widths (typically in the range 5–25 meV for InGaAs/GaAs dots) of the Raman bands. This is partly due to present samples comprising dots filled with a range of electrons and also to variations in the size of dots in a given sample. Thus for a better comparison between theory and experiment there is now a need for more experimental work on better defined arrays of dots or, better still, on single dots.

VII. CONCLUDING REMARKS

In the present paper, we used an effective-mass description of electrons and holes in self-assembled quantum dots, and computed, by means of exact-diagonalization techniques, the wave functions of initial (ground), intermediate, and final states entering the transition amplitude of an inelastic light-scattering process, Eq. (1). Polarized and depolarized Raman cross sections in the backscattering geometry for dots with electron numbers $N_e=2-6$, and harmonic confinement strengths $\hbar\omega_e=20-50$ meV were calculated. The role of collective (charge and spin-density excitations) and single-particle excitations in Raman spectra was stressed. Particularly interesting is the case of open-shell dots, where the spin selection rules do not hold for Raman scattering, and the six-electron dot, where an almost idealized Raman process with transition through a single intermediate resonance can be realized. We found evidence of approximate outgoing resonances in our second-order scheme, without the need of higher-order terms in the scattering amplitude. Existing experimental results were qualitatively analyzed, although their proper description requires further work, for example, on the inclusion of the polaron effect in Raman scattering.

ACKNOWLEDGMENTS

Part of this work was performed using the computing facilities of the Abdus Salam ICTP, Trieste, Italy. The authors acknowledge helpful discussions with B. Aslan and support by the Caribbean Network for Quantum Mechanics, Particles and Fields (ICTP) and by the Programa Nacional de Ciencias Basicas (Cuba).

[1] C. Schuller, *Inelastic Light Scattering of Semiconductor Nanostructures* (Springer, Berlin, 2006).

[2] L. Chu, A. Zrenner, M. Bichler, G. Böhm, and G. Abstreiter, Appl. Phys. Lett. **77**, 3944 (2000).

[3] T. Brocke, M. T. Bootsmann, M. Tews, B. Wunsch, D. Pfannkuche, C. Heyn, W. Hansen, D. Heitmann, and C. Schuller, Phys. Rev. Lett. **91**, 257401 (2003).

[4] B. Aslan, H. C. Liu, M. Korkusinski, P. Hawrylak, and D. J.

Lockwood, Phys. Rev. B **73**, 233311 (2006); J. Nanosci. Nanotechnol. **8**, 789 (2008).
[5] R. P. Miranda, M. I. Vasilevskiy, and C. Trallero-Giner, Phys. Rev. B **74**, 115317 (2006).
[6] E. Menendez-Proupin, C. Trallero-Giner, and S. E. Ulloa, Phys. Rev. B **60**, 16747 (1999).
[7] C. P. Garcia, V. Pellegrini, A. Pinczuk, M. Rontani, G. Goldoni, E. Molinari, B. S. Dennis, L. N. Pfeiffer, and K. W. West, Phys. Rev. Lett. **95**, 266806 (2005).
[8] S. Kalliakos, M. Rontani, V. Pellegrini, C. P. García1, A. Pinczuk, G. Goldoni, E. Molinari, L. N. Pfeiffer, and K. W. West, Nat. Phys. **4**, 467 (2008).
[9] A. Gonzalez and A. Delgado, Physica E **27**, 5 (2005).
[10] O. Madelung, *Semiconductors: Data Handbook* (Birkhauser, Stuttgart, 2004).
[11] R. Loudon, Adv. Phys. **13**, 423 (1964).
[12] A. Delgado, A. Gonzalez, and D. J. Lockwood, Phys. Rev. B **69**, 155314 (2004).
[13] A. Delgado, Ph.D. thesis, Institute of Cybernetics, Mathematics and Physics, Havana, 2006.
[14] L. Jacak, P. Hawrylak, and A. Wojs, *Quantum Dots* (Springer, Berlin, 1998).
[15] Y. Masumoto and T. Takagahara, *Semiconductor Quantum Dots, Physics, Spectroscopy and Applications* (Springer-Verlag, Berlin, 2002).
[16] Z. R. Wasilewski, S. Fafard, and J. P. McCaffrey, J. Cryst. Growth **201-202**, 1131 (1999).
[17] P. Hawrylak and M. Korkusinski, in *Single Quantum Dots*, edited by P. Michler (Springer, Berlin, 2003); P. Hawrylak and M. Korkusinski, in *Single quantum dots: Fundamentals, Applications, and New Concepts*, edited by P. Michler, Topics in Applied Physics, Vol. 90 (Springer-Verlag, Berlin, 2003), pp. 25–92.
[18] M. Rontani, C. Cavazzoni, D. Belluci, and G. Goldoni, J. Chem. Phys. **124**, 124102 (2006).
[19] S. Kvaal, arXiv:0810.2644 (unpublished).
[20] P. Ring and P. Schuck, *The Nuclear Many-Body Problem* (Springer-Verlag, New York, 1980).
[21] A. Delgado, A. Gonzalez, and E. Menendez-Proupin, Phys. Rev. B **65**, 155306 (2002).
[22] J. K. Cullum and R. A. Willoughby, *Lanczos Algorithms for Large Symmetric Eigenvalue Computation* (Birkhauser, Stuttgart, 1985).
[23] A. Delgado, A. Gonzalez, and D. J. Lockwood, Solid State Commun. **135**, 554 (2005).
[24] This fact was already noticed for closed shell (relatively large) etched dots in A. Delgado, A. Gonzalez, and D. J. Lockwood, Phys. Rev. B **71**, 241311(R) (2005).
[25] G. Danan, A. Pinczuk, J. P. Valladares, L. N. Pfeiffer, K. W. West, and C. W. Tu, Phys. Rev. B **39**, 5512 (1989).
[26] R. Strenz, U. Bockelmann, F. Hirler, G. Abstreiter, G. Bohm, and G. Weimann, Phys. Rev. Lett. **73**, 3022 (1994).
[27] D. J. Lockwood, P. Hawrylak, P. D. Wang, C. M. Sotomayor Torres, A. Pinczuk, and B. S. Dennis, Phys. Rev. Lett. **77**, 354 (1996).
[28] C. Schuller, K. Keller, G. Biese, E. Ulrichs, L. Rolf, C. Steinebach, D. Heitmann, and K. Eberl, Phys. Rev. Lett. **80**, 2673 (1998).
[29] C. Steinebach, C. Schuller, and D. Heitmann, Phys. Rev. B **59**, 10240 (1999).
[30] C. Steinebach, C. Schuller, and D. Heitmann, Phys. Rev. B **61**, 15600 (2000).
[31] B. Aslan, private communication.
[32] D. Bougeard, P. H. Tan, M. Sabathil, P. Vogl, G. Abstreiter, and K. Brunner, Physica E **21**, 312 (2004).
[33] B. Aslan, Electron. Lett. **43**, 1162 (2007).